University of Tehran

Earth Observation and Geomatics Engineering

Online ISSN: 2588-4360

Homepage: https://eoge.ut.ac.ir/

Pan-sharpening Solutions for Khayyam Satellite Imagery: A Comparative Study on Pixel-Level Image Fusion Approaches

Farhad Samadzadegan[1], **Ahmad Toosi**[2]✉, **Hadiseh Hasani**[3], and **Omran Amini**[4]

1. School of Surveying and Geospatial Engineering, University College of Engineering, University of Tehran, Tehran, Iran. E-mail: samadz@ut.ac.ir
2. Corresponding author, School of Surveying and Geospatial Engineering, University College of Engineering, University of Tehran, Tehran, Iran. E-mail: ahmadtoosi71@ut.ac.ir
3. Department of Geodesy and Surveying Engineering, Tafresh University, Tafresh, Iran. E-mail: h.hasani@tafreshu.ac.ir
4. Iranian Space Research Center (ISRC), Tehran, Iran. E-mail: Ir.omran.amini@gmail.com

Article Info

Article type:
Research Article

Article history:
Received 2026-01-25
Received in revised form 2026-06-02
Accepted 2026-06-07
Available online 2026-07-24

Keywords:
Remote sensing,
Khayyam satellite,
Pan-sharpening,
Spatial resolution,
Deep learning.

ABSTRACT

Objective: This study presents the first comprehensive evaluation of pan-sharpening methods on Iran's Khayyam satellite imagery, launched in August 2022. **Method**: Twenty-one algorithms across traditional methods (including component substitution, multi-resolution analysis, and hybrid approaches) and advanced deep learning networks were compared using Khayyam data from Yazd-Iran, Semnan-Iran, and Baotou-China, with 0.8-meter panchromatic and 3.2-meter multispectral resolution. Traditional methods included 18 algorithms such as PCA, Gram-Schmidt variants, MTF-GLP methods, wavelet-based approaches, and hybrid combinations of wavelet and Gram-Schmidt techniques. Due to unique spectral characteristics, three deep learning networks (PNN, PanNet, PSGAN) were trained on Khayyam data. Quality assessment was conducted using visual analysis and quantitative metrics, including SAM, ERGAS, SSIM, PSNR, and UIQI for spectral quality, and SCC for spatial quality. **Results**: Results showed that traditional methods like GS-Wavelet and PRACS achieved superior performance with PSNR values exceeding 76 dB and SSIM above 0.99. Deep learning methods showed limited performance despite sensor-specific training, requiring extensive training data specific to Khayyam's sensor characteristics. **Conclusions**: No single method excelled universally, revealing trade-offs between spatial enhancement and spectral preservation. Baseline performance metrics for Khayyam imagery pan-sharpening were established, and insights for optimal method selection were provided.

Cite this article: Samadzadegan, F., Toosi, A., Hasani, H., & Amini, Omran. (2026). Pan-sharpening solutions for Khayyam satellite imagery: A comparative study on pixel-level image fusion approaches, *Earth Observation and Geomatics Engineering*, Volume 10, Issue 1, Pages 29-40. http//doi.org/10.22059/eoge.2026.410000.1212

Publisher: University of Tehran.
DOI: http//doi.org/10.22059/eoge.2026.410000.1212

1. Introduction

A growing number of optical satellite sensors are available on several Earth observation (EO) platforms (Zhao et al., 2022). According to the technical limitations of satellite imaging systems, acquiring multispectral (MS) images with high spatial resolution is impossible. Consequently, most satellites collect panchromatic (Pan) images with high spatial resolution along with MS with high spectral resolution, simultaneously (Xu et al., 2014). To jointly use the spectral and spatial content of MS and Pan images, pan-sharpening methods are developed (Javan et al., 2021). These methods generate an MS image with high spatial resolution by fusing pixel-level data of Pan and MS images.

According to the importance of the pan-sharpening issue, a wide range of methods are adopted to produce high-quality and more accurate fused images (Fazilov et al., 2024; Wang et al., 2024). However, by introducing new generations of very high-resolution (VHR) EO sensors, pan-sharpening has remained a challenging task in remote sensing communities (Ciotola et al., 2022). The Khayyam satellite is one of the newly introduced VHR EO satellites by Iran, which was successfully launched into low Earth orbit in August 2022 (ISA, 2024). The pan-sharpening of Khayyam imagery has not yet been evaluated. This research aims to assess the pan-sharpening methods on Khayyam images and evaluate their performance.

There are two categories of pan-sharpening methods: traditional and advanced deep learning-based methods. Component substitution (CS), multi-resolution analysis (MRA), variational optimization (VO), and hybrid are main groups of traditional methods that are widely applied in remote sensing applications. On the other hand, the success of deep learning methods in various applications leads to the development of several networks also for pan-sharpening purposes.

CS approaches are the most practical and common techniques for pan-sharpening due to their calculation speed. CS techniques map the MS into a new domain based on a transformation that contains the spatial and spectral information. The spatial component is replaced by the Pan image, and the pan-sharpened image is generated based on the inverse transformation (Rahimzadeganasl et al., 2019). Several CS methods are proposed with different transformation matrices, including principle component analysis (PCA) (Kwarteng & Chavez, 1989), Gram-Schmidt (GS) decomposition (C. A. Laben & B. V. Brower, 2000), Brovey transform (Gillespie et al., 1987), and intensity-hue-saturation (IHS) (Tu et al., 2004). Recently generalized CS methods are considered to improve the performance of the original one, such as improved IHS by applying wavelet decomposition (Lari & Yazdi, 2016), improved GS with guided filter (Li et al., 2016), and variational PCA (Zhou et al., 2014). Although CS methods have high speed, simple computation, and the results have high spatial quality, they suffer from spectral distortion (Licciardi et al., 2016).

To address the pan-sharpening approach from a spatial viewpoint, MRA methods are proposed. The most important advantages of this category are its robustness and spectral accuracy (Wang et al., 2023). They decompose images into a sequence with decreasingly informative content. The spatial information of Pan is inserted into MS at the same level. They preserve the spectral information of MS, and they perform better in spectral metrics. The most common MRA methods are wavelet-based (King & Wang, 2001), contourlet (Shah et al., 2007), and morphological filtering (Schavemaker et al., 2000). VO techniques are the third group of traditional pan-sharpening methods. Due to the demand for data-dependent parameters tuning, they have been less applied in comparison with CS and MRA methods (Restaino, 2024). Low-rank representation (Palsson et al., 2019), total variation (Palsson et al., 2013), and filter estimation (Vivone, Simões, et al., 2014) are some VO methods.

During the last decade, deep learning-based pan-sharpening methods have been successfully applied in remote sensing applications (Deng et al., 2022). They designed a non-linear network to reconstruct a high spectral and spatial image based on information from MS and Pan images. For this purpose, several network architectures are evaluated in the literature, such as autoencoder (Huang et al., 2015), fully convolutional neural network (CNN) (Masi et al., 2016), residual deep learning network (N. Li et al., 2017), and generative adversarial network (GAN) (Liu et al., 2020). Although pan-sharpening based on deep learning networks has reached high spectral and spatial accuracy, it requires a huge dataset with available ground-truth and also high computational time.

To benefit from two or more pan-sharpening algorithms, some researchers focus on the combination of pan-sharpening approaches (Akula et al., 2012; Wady et al., 2020). The hybrid approaches may use traditional algorithms such as PCA and contourlet (Akula et al., 2012), IHS and wavelet (Wady et al., 2020), and GS and curvelet transform (Hammad et al., 2021). Moreover, some traditional pan-sharpening algorithms are applied to improve deep learning networks, including PCA and CNN (Guarino et al., 2023) and deep learning and multi-resolution representation (Huang et al., 2020).

Various pan-sharpening approaches have been implemented in remote sensing applications on different satellite images. The spectral response and ground sampling distance (GSD) of Khayyam images differ from other satellite imagery. Since the potential of pan-sharpening methods on Khayyam imagery has not been assessed yet, a comparative study of pan-sharpening methods on Khayyam images is performed in this article.

The Khayyam satellite is Iran's first VHR EO satellite, successfully launched into low Earth orbit in August 2022. It operates in a Sun-synchronous orbit at a mean altitude of 500 km with a local time of ascending node of 10:30, enabling an average global revisit time of four days. The spacecraft features an agile platform designed for fast and precise off-nadir imaging capabilities (up to ±40°). It carries a push-broom high-resolution optical imaging sensor with five spectral bands (one Pan and four MS) and provides 12-bit radiometric resolution. The GSDs of Pan and MS bands are 0.8 and 3.2 meters, respectively (ISA, 2024; Samadzadegan et al., 2025).

2. Related works

During the last four decades, several pan-sharpening methods have been presented for satellite imagery (Javan et al., 2021). Vivone et al. (2014) provided a critical description and comparison of CS and MRA methods. The analysis of algorithms' behaviors was evaluated at full and reduced resolutions. For this purpose, five datasets from different satellite images were considered for the evaluation process. CS methods generated a fused image with fewer aliasing impairments, along with robustness to misregistration of MS and Pan. MRA methods had good overall performance and can be applied to multi-platform data fusion (Vivone, Alparone, et al., 2014).

H. Li et al. (2017) compared four CS and four MRA methods on WorldView (WV)-2 based on information indices, image quality metrics, and visual inspection. The experimental results on six images showed that the generalized Laplacian pyramid is a suitable method for the pan-sharpening of WV-2 images for applications of building, water-bodies, and vegetation extraction. Pushparaj and Hegde (2017) presented twelve CS, MRA, and hybrid methods on QuickBird-2 imagery. The results of the spectral quality metrics depicted that Ehlers method better preserves the spectral information. From a spatial perspective, the Fuse Go method had the best performance. Kahraman and Ertürk (2017) compared the performance of fifteen traditional pan-sharpening methods on GÖKTÜRK-2 imagery. The assessment results depicted that partial replacement adaptive component substitution as CS methods and smoothing filter-based intensity modulation as MRA methods had the highest metrics.

Kim et al. (2018) evaluated four CS and MRA methods on Pleiades 1A and KOMPSAT 3 satellite images. Analyzing the fused images visually and also based on quantitative indices showed that for Pleiades 1A, adopting GS had better spatial performance and less spectral distortion. Moreover, the best performance on KOMPSAT-3 was for smoothing filter-based intensity modulation and adopting GS methods.

Govind et al. (2019) evaluated four CS and MRA methods on Landsat-8 in the urban area. To assess the fused image, four indices have been applied. The obtained results showed that the pan-sharpened image based on modified HIS had better visual quality. Moreover, the high-pass filter method gained the best quantitative metric values. Alcaras et al. (2021) applied eight CS pan-sharpening methods on IKONOS imagery. The results showed that the simple mean and multiplicative lead spectral distortion. On the other hand, GS fast had the best performance among the eight approaches.

Alcaras and Parente (2023) evaluated the potential of pan-sharpening methods in GeoEye-1 imagery on different land cover types. Four areas, including natural, rural, urban, and semi-urban, were considered. Nine traditional pan-sharpening methods were compared. The results proved that Brovey had the best performance among the implemented methods. Wu et al. (2023) sharpened all Sentinel-2 images into 10-meter resolution based on a hierarchical fusion network. The performance of the proposed method was compared with several traditional and deep learning-based methods. The fused image had an improvement in spatial information while preserving spectral information.

In recent years, increasingly diverse deep learning networks have been implemented to fuse Pan and MS images in the literature (He et al., 2025). Masi et al. (2016) proposed a three-layer convolutional network initially for IKONOS, GeoEye-1, and WV-2 images pan-sharpening. Data augmentation was performed by non-linear radiometric mapping. The results were compared with basic networks, which proved the ability of the proposed method. Furthermore, several advancements have been introduced in more complex networks. Generally, the common deep learning methods in this field are residual networks (Wang et al., 2022), transformers (Su et al., 2022), attention-based networks (Jia et al., 2024), and GAN (Liu et al., 2020).

The literature review suggests that there is no unique method for pan-sharpening with the best performance on most satellite images. Consequently, with the emergence of the high-resolution satellite imagery new generation, comprehensive and comparative analysis is required for its pan-sharpening evaluation. The potential of pan-sharpening methods on the Khayyam image has not yet been assessed in the literature.

3. Material and methods

3.1. Dataset

The dataset used in this study consists of Khayyam satellite imagery acquired over Meybod, Yazd Province, Iran; Aradan, Semnan Province, Iran; and Baotou, Inner Mongolia, China. The Pan band was cropped to a 2048×2048 pixel square subset, while the corresponding MS bands (red, green, blue, and NIR) have dimensions of 512×512 pixels, maintaining the 1:4 spatial resolution ratio between Pan and MS bands. The MS bands provide a GSD of 3.2 meters, while the Pan band offers 0.8-meter resolution. To enhance inter-band alignment, sub-pixel-level band-to-band co-registration was applied.

To meet the extensive training data requirements of deep learning methods, all these datasets were used to ensure sufficient samples for robust deep learning model development. The spatial and spectral diversity of these locations provides comprehensive training coverage for the neural networks. For traditional methods, the MS and Pan images for each case study were treated as algorithm inputs separately. Figure 1 presents representative samples from all three datasets used in this evaluation.

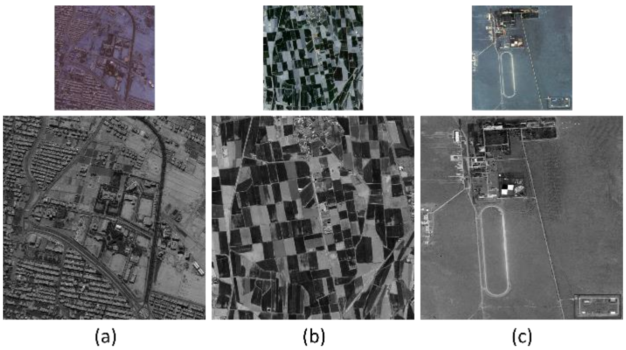

Figure 1. Sample Khayyam dataset: (a) Meybod, Iran; (b) Semnan, Iran; and (c) Baotou, China. Upper images: MS; lower images: Pan.

3.2. Pan-sharpening methods

A set of 21 pan-sharpening algorithms was selected for evaluation, spanning two main categories: traditional methods and deep learning networks. The traditional methods were further subdivided into CS techniques including Brovey (Gillespie et al., 1987), PCA (Jiang et al., 2011), Ehlers (Klonus & Ehlers, 2009), Generalized IHS (GIHS) (Tu et al., 2001), GS (C. Laben & B. Brower, 2000), High Pass Filter (HPF) (Chavez et al., 1991), Indusion, Partial Replacement Adaptive Component Substitution (PRACS) (Vivone, Alparone, et al., 2014), and Smoothing Filter-based Intensity Modulation (SFIM) (Liu, 2000); MRA methods comprising Morphological Half Gradient (MF-HG) (Restaino et al., 2016), Modulation Transfer Function- Generalized Laplacian Pyramid (MTF-GLP) (Aiazzi et al., 2002; Aiazzi et al., 2006), MTF-GLP-Context-Based Decision (MTF-GLP-CBD) (Aiazzi et al., 2002; Aiazzi et al., 2006; Aiazzi et al., 2007), MTF-GLP with Enhanced Context-Based model (MTF-GLP-ECB) (Aiazzi et al., 2002; Aiazzi et al., 2006; Aiazzi et al., 2007), MTF-GLP with High-Pass Modulation model (MTF-GLP-HPM) (Aiazzi et al., 2003; Aiazzi et al., 2006), and Wavelet (Amolins et al., 2007); and Hybrid approaches included Additive Wavelet Intensity (AWI) (Nunez et al., 1999) and GS-Wavelet (Javan et al., 2021). Additionally, three deep learning networks were implemented: PNN (Masi et al., 2016), PanNet (Yang et al., 2017), and PSGAN (Liu et al., 2020).

Since pre-trained deep learning models available in the literature are typically trained on datasets from other satellite systems, they are incompatible with Khayyam data due to significant differences in spatial resolution and spectral characteristics. Therefore, all three deep learning networks were trained from scratch using the Khayyam datasets described previously. The trained models were then applied to pansharpen 2048×2048 pixel images, maintaining consistency with the input data used for traditional method evaluation. This approach ensures fair comparison across all methodological categories while accounting for the unique sensor characteristics of the Khayyam satellite system.

3.3. Quality assessment methods

Quality assessment was conducted using two approaches: qualitative and quantitative. Qualitative assessment involved visual inspection and comparison of pansharpened results to identify superior methods based on visual criteria such as spatial detail preservation, spectral consistency, and artifact presence.

Quantitative assessment employed established image quality metrics to objectively compare pansharpened images against reference data. For spatial evaluation, pansharpened images were compared with the Pan image. Spectral assessment involved comparison with the MS images to evaluate spectral fidelity and distortion levels. Metrics included spectral measures (Spectral Angle Mapper (SAM), Relative Dimensionless Global Error in Synthesis (ERGAS), Structural Similarity Index Measure (SSIM), Universal Image Quality Index (UIQI), Peak Signal-to-Noise Ratio (PSNR)) and spatial measures (SCC) (Table 1). Due to the absence of true reference images at full resolution, evaluation was performed using the pseudo-reference scheme based on Wald's protocol (Wald et al., 1997).

Table 1. Quality assessment metrics*.

Metric formula	Reference
$\mathrm{SAM(MS,F)}=\arccos\left[\frac{\sum_{i=1}^{n}(\mathrm{MS}(i)\text{-}\mathrm{F}(i))}{\sqrt{\sum_{i=1}^{n}\mathrm{MS}(i)}\sqrt{\sum_{i=1}^{n}\mathrm{F}(i)}}\right]$ (1)	(Alparone et al., 2007)
$\mathrm{ERGAS}=100\frac{\mathrm{GSD_F}}{\mathrm{GSD_{MS}}}\sqrt{\frac{1}{n}\sum_{j=1}^{n}\left(\frac{\mathrm{RMSE}(b_i)}{\mu_i}\right)^2}$ (2)	(Wald, 2000)
$\mathrm{PSNR(MS,F)}=20\log_{10}\left(\frac{L^2}{\frac{1}{MN}\sum_{i=1}^{M}\sum_{j=1}^{N}(\mathrm{MS}(i,j)\text{-}\mathrm{F}(i,j))^2}\right)$ (3)	(Gonzalez, 2009)
$\mathrm{UIQI(MS,F)}=\frac{4\sigma_{MS,F}(\mu_{MS}+\mu_F)}{(\sigma^2MS+\sigma^2F)(\mu^2MS+\mu^2F)}$ (4)	(Wang & Bovik, 2002)
$\mathrm{SSIM(MS,F)}=\frac{(2\mu_{MS}\mu_F+C1)(2\sigma_{MS,F}+C2)}{(\mu^2MS+\mu^2F+C1)(\sigma^2MS+\sigma^2F+C1)}$ (5)	(Wang et al., 2004)
$\mathrm{SCC(Pan,F)}=\mathrm{CC}(\mathrm{Edge_F},\mathrm{Edge_{Pan}})$ (6)	(Ehlers et al., 2010)

* F: fused image; n: number of bands; M and N: image dimensions; L: dynamic range of the image; μ: mean; σ: standard deviation; σ^2: covariance; C_1 and C_2: constants; Edge: edge-extracted images; CC: correlation coefficient. The ideal value for SAM is 0 (range is 0 to 90 degrees); for ERGAS the ideal value is 0 (lower values indicate better quality); for PSNR higher values indicate better quality; for UIQI and SSIM the ideal value is 1 (range is 0 to 1); for SCC the ideal value is 1 (range is -1 to 1, with higher values indicating better spatial correlation).

3.4. Experimental framework

The experimental framework consists of four stages: data preparation, algorithm implementation, quality assessment, and comparative analysis (Figure 2). In the data preparation stage, Khayyam satellite imagery from three geographical locations was preprocessed to ensure consistency. Band-to-band co-registration was applied to enhance inter-band alignment between Pan and MS images. The Pan band was cropped to 2048×2048 pixel subsets, while MS bands were maintained at 512×512 pixels, preserving the 1:4 spatial resolution ratio characteristic of Khayyam's sensor specifications.

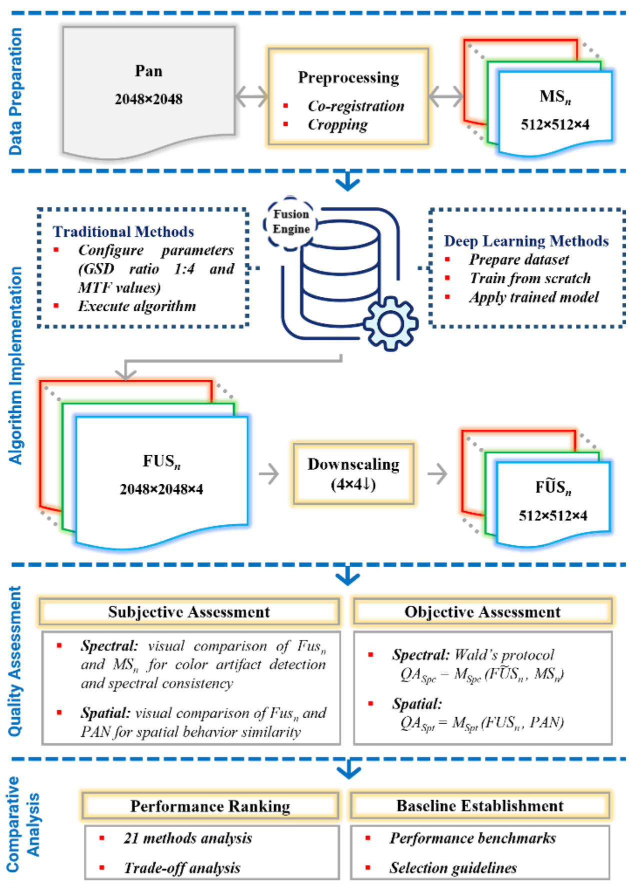

Figure 2. Flowchart of the experimental framework.

For algorithm implementation, traditional pan-sharpening methods were executed with parameters configured according to Khayyam's specific sensor characteristics, including the GSD ratio of 1:4 and sensor-specific MTF values. Deep learning networks required a distinct implementation pipeline: training datasets were generated through patch extraction and augmentation from all three geographical locations, models were trained from scratch using GPU-accelerated TensorFlow framework, and the trained models were subsequently applied to full-resolution 2048×2048 pixel images for pan-sharpening.

Quality assessment was conducted using Wald's protocol. The pansharpened results were then evaluated against the reference images using both spectral quality metrics and spatial quality metrics. Visual analysis complemented the quantitative assessment to identify artifacts, spectral distortions, and spatial enhancement characteristics. Finally, comparative analysis integrated quantitative metrics and visual inspection results to rank algorithm performance, identify method-specific strengths and limitations, and establish baseline performance benchmarks for Khayyam imagery pan-sharpening.

3.5. System configurations

Implementation was carried out using a laptop system equipped with an AMD Ryzen 7 5800H CPU (3.20 GHz), an NVIDIA GeForce RTX 3060 8GB GPU, and 32GB of system RAM. Deep learning methods were implemented in Python using the TensorFlow framework, leveraging GPU acceleration for model training and inference. Traditional pan-sharpening algorithms were executed using the MATLAB R2021a environment.

4. Results and discussions

Traditional pan-sharpening algorithms were configured with parameters specifically customized for Khayyam satellite data characteristics. The primary parameters include the GSD ratio between Pan and MS bands, and the modulation transfer function (MTF) values at the Nyquist frequency measured at the field of view (FOV) center. The GSD ratio of 1:4 between Pan and MS bands is consistent with most VHR satellite imagery systems, facilitating algorithm adaptation. The MTF values specific to Khayyam's sensor were determined for each spectral band: Pan (7.4%), NIR (25.0%), red (27.1%), green (26.7%), and blue (26.9%). These sensor-specific MTF characteristics are crucial for optimal performance of MRA methods and ensure accurate spatial frequency modeling in the pan-sharpening process.

All deep learning networks were trained from scratch using the Khayyam datasets, as transfer learning from existing pre-trained models was not feasible. The pre-trained networks available in the literature are typically trained on other satellite imagery systems (e.g., WV), which possess significantly different spatial resolution and spectral characteristics compared to Khayyam data. These fundamental differences in sensor specifications prevent effective knowledge transfer and necessitate sensor-specific training.

For training, all available datasets were used to ensure sufficient data diversity and volume for robust model development. The configurations and hyperparameters for the three deep learning methods are reported in Table 2, with parameters set based on source papers and empirical optimization for this case study. Figure 3 illustrates the training loss evolution for three methods, demonstrating convergence behavior and training stability achieved during the model development process.

Table 2. Configuration parameters and architectural specifications for deep learning-based pan-sharpening networks.

Parameter/ method	PanNet	PNN	PSGAN
Patch Size	32×32	32×32	64×64
Architecture Type	Dual-branch with adaptive fusion	Parallel processing	Generative Adversarial Network
MS Branch Layers	Conv2D: 64(3×3), 32(3×3), 4(3×3)	Conv2D: 64(9×9), 32(5×5), 4(5×5)	Encoder: 64(3×3), 128(3×3), 256(3×3)
Pan Branch Layers	Conv2D: 64(3×3), 32(3×3), 4(3×3)	Conv2D: 64(9×9), 32(5×5), 4(5×5)	Encoder: 64(3×3), 128(3×3), 256(3×3)
Fusion Method	Adaptive weighting + residual	Direct addition	Adversarial training
Optimizer	Adam (lr=0.001)	Adam (lr=0.001)	Adam (lr=0.0001)
Batch Size	8	2	16
Training Epochs	100	100	100
Base Patches	8,000	8,000	8,000
Augmentation Factor	4× (32,000 total)	4× (32,000 total)	4× (32,000 total)
Loss Function	Custom (MSE + gradient)	MSE	L1 content + adversarial (100:1 ratio)
Activation Functions	ReLU, Sigmoid (output)	ReLU, Sigmoid (output)	ReLU, LeakyReLU (discriminator)
Special Features	High-pass filtering, residual learning	Simple architecture	GAN framework, attention mechanism

The results of 21 pan-sharpening methods along with Pan and MS images are shown in Figure 4. Note that for the sake of brevity, only the results of the Meybod case are presented as an example. The comprehensive evaluation of pan-sharpening methods on Khayyam satellite imagery reveals significant performance variations across different algorithmic categories, as demonstrated through both visual analysis (Figure 4) and quantitative assessment (Table 3).

The quantitative metrics identify GS-Wavelet and PRACS as the top-performing algorithms across multiple evaluation criteria. GS-Wavelet and PRACS emerged as top performers across multiple evaluation criteria. GS-Wavelet achieved exceptional spectral preservation while maintaining good spatial correlation. PRACS demonstrated similarly superior spectral quality, though with lower spatial correlation.

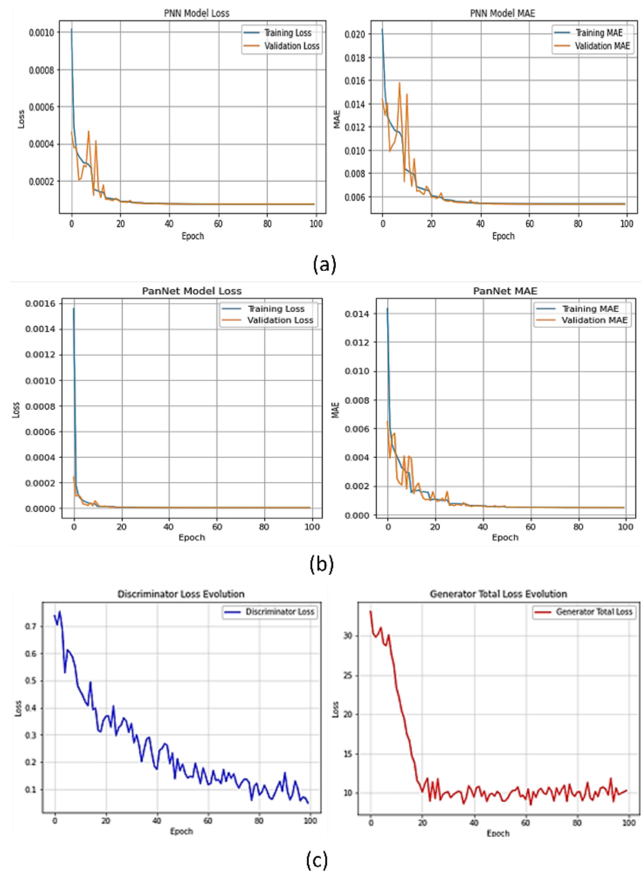

Figure 3. Training loss evolution for deep learning-based pan-sharpening methods: (a) PNN, (b) PanNet, and (c) PSGAN.

Among CS approaches, Brovey achieved reasonable spectral quality but moderate spectral distortion, while providing acceptable spatial correlation. PCA and GS demonstrated balanced performance with good spectral preservation and reasonable spatial enhancement. Notably, Indusion showed excellent spectral preservation but severely compromised spatial quality, highlighting the fundamental trade-off in CS methods. The MRA methods exhibit varying degrees of success. Standard Wavelet achieves good spectral preservation with acceptable spatial metrics. However, MTF-GLP variants show dramatically different performance levels. While MTF-GLP-HPM maintains reasonable quality, MTF-GLP-CBD and MTF-GLP-ECB demonstrate extremely poor performance with SAM values exceeding 7 and ERGAS values above 7, indicating severe spectral and spatial distortions.

The deep learning approaches show concerning underperformance compared to traditional methods. PNN and PanNet achieve similar but poor results with PSNR values around 26 dB and SSIM below 0.85, indicating significant quality degradation. PSGAN performs marginally better but still falls considerably short of traditional methods. The consistently low SCC values across all deep learning methods suggest poor spatial correlation preservation.

Table 3. Quantitative quality assessment results.

Method /metric	SAM	ERGAS	SSIM	PSNR	UIQI	SCC
AWI	0.557	2.002	0.966	66.806	0.953	0.895
Brovey	0.176	2.747	0.980	70.200	0.938	0.680
Ehlers	0.617	2.442	0.966	63.387	0.930	0.917
GIHS	0.628	2.228	0.974	63.939	0.956	0.896
GS	0.682	2.198	0.976	63.849	0.955	0.893
GS-Wavelet	0.402	1.076	0.993	76.531	0.989	0.848
HPF	1.327	4.350	0.887	58.610	0.903	0.845
Indusion	0.176	2.968	0.988	58.305	0.985	0.368
MF-HG	1.113	3.750	0.881	65.016	0.904	0.866
MTF-GLP	1.656	3.208	0.907	64.352	0.926	0.865
MTF-GLP-CBD	10.890	10.744	0.658	59.436	0.601	0.860
MTF-GLP-ECB	7.347	7.383	0.740	56.518	0.752	0.842
MTF-GLP-HPM	0.988	3.296	0.907	68.158	0.922	0.930
PanNet	0.308	11.112	0.842	26.131	0.875	0.371
PCA	0.735	2.171	0.975	64.600	0.956	0.890
PNN	0.528	11.089	0.824	26.136	0.875	0.365
PRACS	1.011	1.191	0.992	76.6405	0.989	0.501
PSGAN	0.352	11.171	0.958	38.061	0.910	0.366
SFIM	0.875	4.531	0.886	61.540	0.899	0.840
Wavelet	2.355	1.733	0.970	68.409	0.971	0.605
WWI	0.530	1.919	0.972	67.560	0.956	0.902

* Red: CS, Blue: MRA, Purple: hybrid, and Green: deep learning

The visual analysis of Figure 4 corroborates the quantitative findings. Brovey demonstrates enhanced spatial sharpness but exhibits noticeable spectral distortion. PRACS stands out among CS methods, delivering excellent spatial detail preservation with minimal spectral artifacts. PCA maintains better spectral consistency while providing reasonable spatial enhancement. MRA methods exhibit their characteristic spectral preservation strength. MTF-GLP-HPM shows good spatial detail preservation, particularly in boundary areas, aligning with its superior spatial correlation. Conversely, MTF-GLP-CBD and MTF-GLP-ECB demonstrate poor visual quality with artifacts, corresponding to their poor quantitative performance.

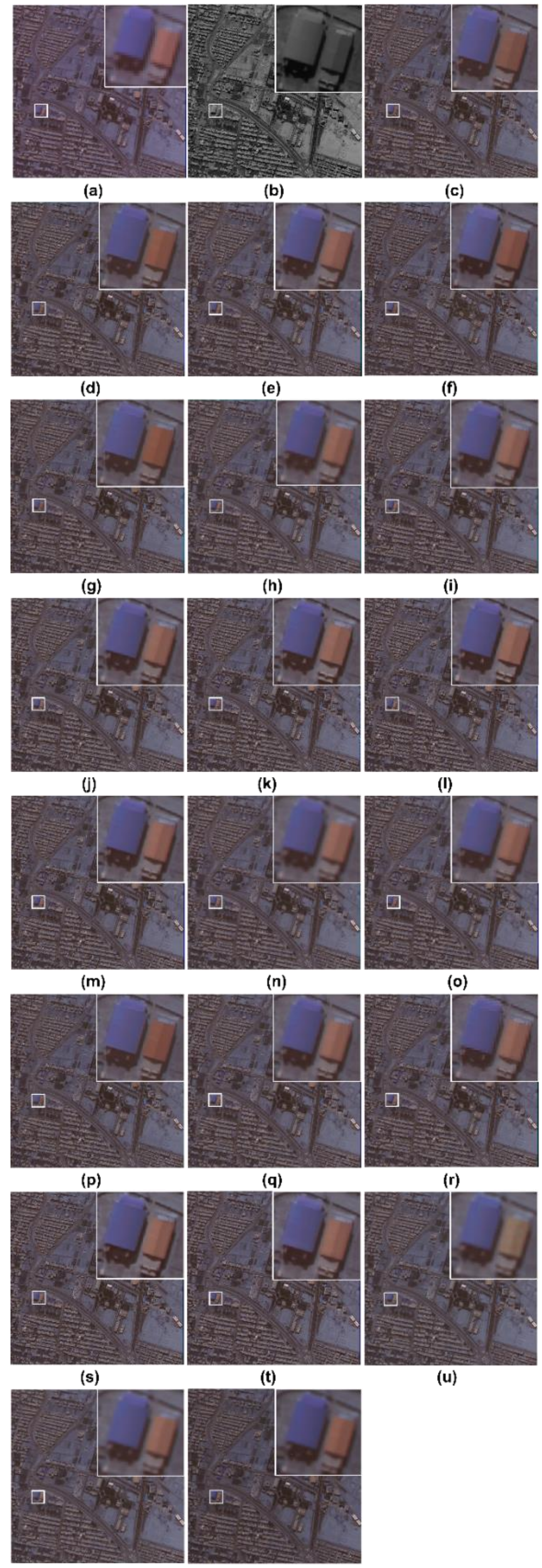

Figure 4. Pan-sharpening results in Meybod dataset: (a) MS, (b) PAN, (c) Brovey, (d) PCA, (e) WWI, (f) Ehlers, (g) GS, (h) PRACS, (i) SFIM, (j) MTF-GLP, (k) MTF-GLP-CBD, (l) MTF-GLP-ECB, (m) MTF-GLP-HPM, (n) Indusion, (o) GS-Wavelet, (p) GIHS, (q) HPF, (r) Wavelet, (s) MF-HG, (t) AWI, (u) PNN, (v) PanNet, (w) PSGAN.

Wavelet maintains excellent spectral fidelity with reasonable spatial enhancement. GS-Wavelet achieves optimal visual quality, successfully combining spatial enhancement with spectral preservation across different land cover types. This superior performance directly corresponds to its good quantitative metrics across all evaluation criteria. Deep learning methods show concerning visual artifacts. PNN and PanNet introduce visible artifacts in homogeneous areas, explaining their poor quantitative scores. PSGAN demonstrates better texture preservation but inconsistent performance across land cover types.

The results reveal distinct trade-off patterns. CS methods generally favor spatial enhancement at the expense of spectral fidelity, evident in methods showing good spatial correlation but higher spectral distortion. MRA methods typically preserve spectral information better, achieving excellent spectral quality while maintaining reasonable spatial enhancement. Hybrid methods demonstrate benefits by combining complementary strengths. GS-Wavelet achieves optimal balance by merging GS's spatial capabilities with wavelet spectral preservation, resulting in top-tier performance. This suggests hybrid methods are well-suited for Khayyam imagery applications.

The poor deep learning performance highlights the critical importance of sensor-specific training data. Despite Khayyam-specific training, these methods struggle to match traditional performance, likely due to limited training dataset size and unique spectral characteristics. This represents a limitation for operational pan-sharpening applications with new sensor systems.

A more careful visual inspection of Figure 4 indicates clear differences in how the methods reconstruct edges, textures, and color consistency. GS-Wavelet and PRACS provide visually balanced results, preserving sharp boundaries of agricultural parcels and built structures while maintaining colors close to the original multispectral image. Brovey produces stronger contrast and sharper appearance, but some regions appear overly enhanced relative to the reference MS image. PCA and GS generate comparatively natural colors, although the spatial sharpening is less pronounced than in GS-Wavelet. The MTF-GLP-CBD and MTF-GLP-ECB results show obvious visual degradation, with noticeable color distortion and reduced image naturalness, consistent with their weak quantitative scores. Among the deep learning methods, PNN and PanNet appear smoother and less detailed than the best traditional methods, especially in fine structures and field boundaries, while PSGAN recovers relatively better texture but still does not reach the visual quality of GS-Wavelet or PRACS. Overall, Figure 4 shows that the most successful methods are those that enhance edges and fine structures without introducing visible spectral distortion or unnatural contrast changes.

Spectral signature preservation analysis (Figure 5) reveals critical differences in maintaining MS band characteristics. GS-Wavelet, PRACS, and standard Wavelet demonstrate excellent spectral fidelity, closely matching original MS signatures across all bands. Conversely,

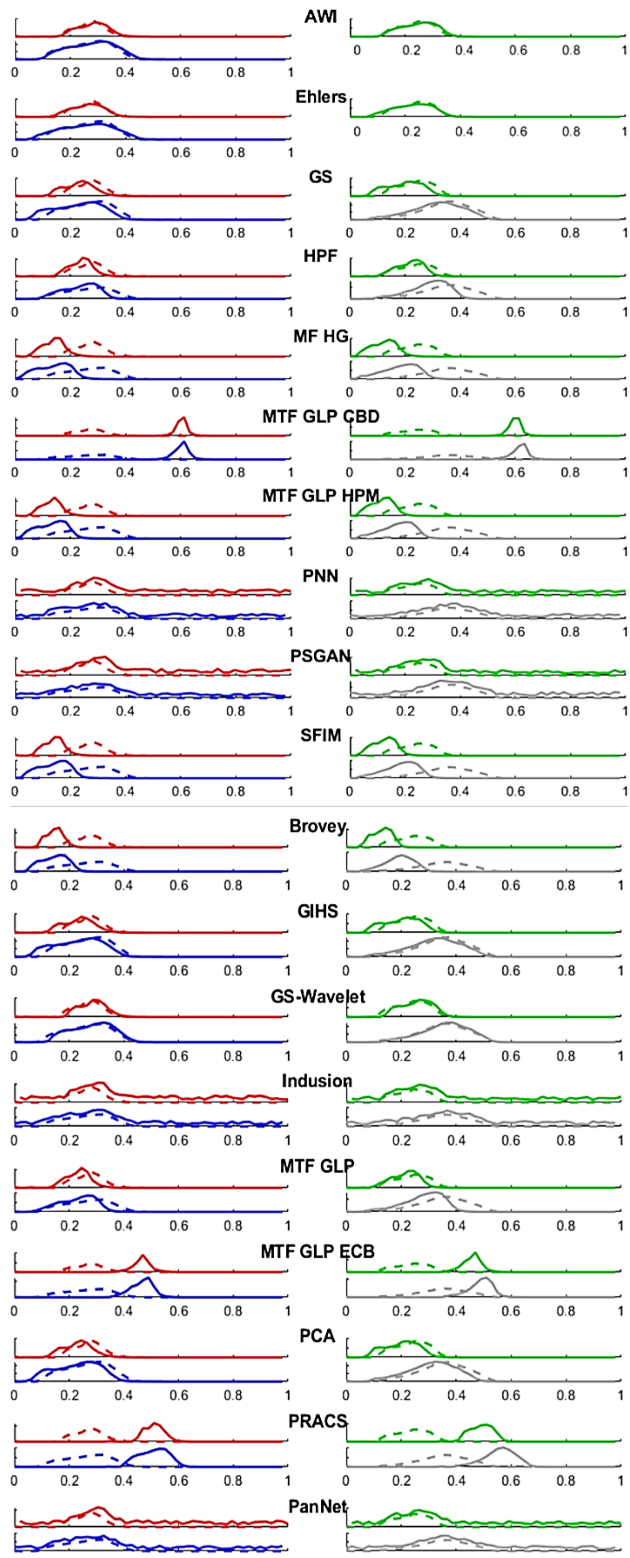

Figure 5. Spectral signature preservation analysis using histogram correlation (Solid and dashed lines represent MS and pansharpened images, respectively. Red, blue, green, and gray lines correspond to red, blue, green, and NIR bands, respectively).

methods like MTF-GLP-CBD and MTF-GLP-ECB show severe spectral deviations, particularly in NIR and red bands, explaining their poor ERGAS and SAM scores. Deep learning methods exhibit moderate spectral preservation but with noticeable deviations in specific spectral regions, highlighting their limitation in maintaining the original spectral information that is crucial for remote sensing applications.

5. Conclusions

This study presents the first comprehensive evaluation of pan-sharpening methods on Khayyam imagery, establishing baseline performance metrics for this VHR EO system. Twenty-one algorithms across traditional and advanced deep learning approaches were compared using the Khayyam dataset. Results demonstrate that hybrid methods outperform deep learning approaches. GS-Wavelet achieved optimal performance, followed by PRACS. Deep learning methods showed poor performance despite sensor-specific training, highlighting adaptation challenges to new sensor characteristics.

The evaluation revealed distinct trade-offs between spatial and spectral quality across method categories. CS methods favored spatial enhancement while MRA methods better preserved spectral information. Hybrid methods successfully balanced both aspects, proving most suitable for Khayyam imagery processing.

Method performance varied across different evaluation criteria, emphasizing the importance of application-specific selection. No single method excelled universally, revealing inherent trade-offs between spatial enhancement and spectral preservation. These findings provide crucial guidance for optimal pan-sharpening strategy selection and establish performance benchmarks for future algorithm development on Khayyam imagery. Future research could focus on evaluating advanced deep learning methods trained with extensive Khayyam imagery datasets to better assess their potential for this satellite system.

Acknowledgements

We sincerely thank the Iranian Space Research Center (ISRC) for providing us with the Khayyam satellite data.

References

Aiazzi, B., Alparone, L., Baronti, S., & Garzelli, A. (2002). Context-driven fusion of high spatial and spectral resolution images based on oversampled multiresolution analysis. IEEE Transactions on Geoscience and Remote Sensing, 40(10), 2300-2312. https://doi.org/10.1109/TGRS.2002.803623

Aiazzi, B., Alparone, L., Baronti, S., Garzelli, A., & Selva, M. (2003). An MTF-based spectral distortion minimizing model for pan-sharpening of very high resolution multispectral images of urban areas. 2003 2nd GRSS/ISPRS Joint Workshop on Remote Sensing and Data Fusion over Urban Areas. https://doi.org/10.1109/DFUA.2003.1219964

Aiazzi, B., Alparone, L., Baronti, S., Garzelli, A., & Selva, M. (2006). MTF-tailored multiscale fusion of high-resolution MS and Pan imagery. Photogrammetric Engineering & Remote Sensing, 72(5), 591-596. https://doi.org/10.14358/PERS.72.5.591

Aiazzi, B., Baronti, S., & Selva, M. (2007). Improving component substitution pansharpening through multivariate regression of MS $+ $ Pan data. IEEE Transactions on Geoscience and Remote Sensing, 45(10), 3230-3239. https://doi.org/10.1109/TGRS.2007.901007

Akula, R., Gupta, R., & Devi, M. V. (2012). An efficient PAN sharpening technique by merging two hybrid approaches. Procedia Engineering, 30, 535-541. https://doi.org/10.1016/j.proeng.2012.01.895

Alcaras, E., Della Corte, V., Ferraioli, G., Martellato, E., Palumbo, P., Parente, C., & Rotundi, A. (2021). Comparison of different pan-sharpening methods applied to IKONOS imagery. Geogr. Tech, 16, 198-210. https://doi.org/10.21163/GT_2021.163.15

Alcaras, E., & Parente, C. (2023). The effectiveness of pan-sharpening algorithms on different land cover types in geoeye-1 satellite images. Journal of Imaging, 9(5), 93. https://doi.org/10.3390/jimaging9050093

Alparone, L., Wald, L., Chanussot, J., Thomas, C., Gamba, P., & Bruce, L. M. (2007). Comparison of pansharpening algorithms: Outcome of the 2006 GRS-S data-fusion contest. IEEE Transactions on Geoscience and Remote Sensing, 45(10), 3012-3021. https://doi.org/10.1109/TGRS.2007.904923

Amolins, K., Zhang, Y., & Dare, P. (2007). Wavelet based image fusion techniques—An introduction, review and comparison. ISPRS journal of photogrammetry and remote sensing, 62(4), 249-263. https://doi.org/10.1016/j.isprsjprs.2007.05.009

Chavez, P., Sides, S. C., & Anderson, J. A. (1991). Comparison of three different methods to merge multiresolution and multispectral data- Landsat TM and SPOT panchromatic. Photogrammetric Engineering and remote sensing, 57(3), 295-303. https://doi.org/0099-1112/91/5703-295$03.00/0

Ciotola, M., Vitale, S., Mazza, A., Poggi, G., & Scarpa, G. (2022). Pansharpening by convolutional neural networks in the full resolution framework. IEEE Transactions on Geoscience and Remote Sensing, 60, 1-17. https://doi.org/10.48550/arXiv.2111.08334

Deng, L.-J., Vivone, G., Paoletti, M. E., Scarpa, G., He, J., Zhang, Y., Chanussot, J., & Plaza, A. (2022). Machine learning in pansharpening: A benchmark, from shallow to deep networks. IEEE Geoscience and Remote Sensing Magazine, 10(3), 279-315. https://doi.org/10.1109/MGRS.2022.3187652

Ehlers, M., Klonus, S., Johan Åstrand, P., & Rosso, P. (2010). Multi-sensor image fusion for pansharpening in remote sensing. International Journal of Image and Data Fusion, 1(1), 25-45. https://doi.org/10.1080/19479830903561985

Fazilov, S., Yusupov, O., Radjabov, S., Eshonqulov, E., & Abdieva, K. (2024). Analysis of pansharpening methods for multispectral satellite imagery. AIP Conference Proceedings. https://doi.org/10.1063/5.0241414

Gillespie, A. R., Kahle, A. B., & Walker, R. E. (1987). Color enhancement of highly correlated images. II. Channel ratio and “chromaticity” transformation techniques. Remote Sensing of Environment, 22(3), 343-365. https://doi.org/10.1016/0034-4257(87)90088-5

Gonzalez, R. C. (2009). Digital image processing. Pearson education india.

Govind, N. R., Rishikeshan, C., & Ramesh, H. (2019). Comparison of different pan sharpening techniques using Landsat 8 imagery. 2019 IEEE 5th International Conference for Convergence in Technology (I2CT). https://doi.org/10.1109/I2CT45611.2019.9033659

Guarino, G., Ciotola, M., Vivone, G., Poggi, G., & Scarpa, G. (2023). PCA-CNN hybrid approach for hyperspectral pansharpening. IEEE Geoscience and Remote sensing letters, 20, 1-5. https://doi.org/10.1109/LGRS.2023.3326204

Hammad, M., Ghoniemy, T., Mahmoud, T., & Amein, A. (2021). Hybrid fusion using Gram Schmidt and Curvelet transforms for satellite images. IOP Conference Series: Materials Science and Engineering. https://doi.org/10.1088/1757-899X/1172/1/012016

He, X., Cao, K., Zhang, J., Yan, K., Wang, Y., Li, R., Xie, C., Hong, D., & Zhou, M. (2025). Pan-mamba: Effective pan-sharpening with state space model. Information Fusion, 115, 102779. https://doi.org/10.1016/j.inffus.2024.102779

Huang, W., Fei, X., Feng, J., Wang, H., Liu, Y., & Huang, Y. (2020). Pan-sharpening via multi-scale and multiple deep neural networks. Signal Processing: Image Communication, 85, 115850. https://doi.org/10.1016/j.image.2020.115850

Huang, W., Xiao, L., Wei, Z., Liu, H., & Tang, S. (2015). A new pan-sharpening method with deep neural networks. IEEE Geoscience and Remote sensing letters, 12(5), 1037-1041. https://doi.org/10.1109/LGRS.2014.2376034

ISA. (2024). KHAYYAM Imagery User Guide. In I. S. A. (ISA) (Ed.).

Javan, F. D., Samadzadegan, F., Mehravar, S., Toosi, A., Khatami, R., & Stein, A. (2021). A review of image fusion techniques for pan-sharpening of high-resolution satellite imagery. ISPRS journal of photogrammetry and remote sensing, 171, 101-117. https://doi.org/10.1016/j.isprsjprs.2020.11.001

Jia, Y., Hu, Q., Dian, R., Ma, J., & Guo, X. (2024). PAPS: Progressive attention-based pan-sharpening. IEEE/CAA Journal of Automatica Sinica, 11(2), 391-404. https://doi.org/10.1109/JAS.2023.123987

Jiang, D., Zhuang, D., Huang, Y., & Fu, J. (2011). Survey of multispectral image fusion techniques in remote sensing applications. Image fusion and its applications, 1, 1-22. https://doi.org/10.5772/10548

Kahraman, S., & Ertürk, A. (2017). A comprehensive review of pansharpening algorithms for Göktürk-2 satellite images. ISPRS Annals of the Photogrammetry, Remote Sensing and Spatial Information Sciences, 4, 263-270. https://doi.org/10.5194/isprs-annals-IV-4-W4-263-2017

Kim, Y., Choi, J., & Kim, Y. (2018). Image fusion methods for multispectral and panchromatic images of Pleiades and KOMPSAT 3 Satellites. Journal of the Korean Society of Surveying, Geodesy, Photogrammetry and Cartography, 36(5), 413-422. https://doi.org/10.7848/ksgpc.2018.36.5.413

King, R. L., & Wang, J. (2001). A wavelet based algorithm for pan sharpening Landsat 7 imagery. IGARSS 2001. Scanning the Present and Resolving the Future. Proceedings. IEEE 2001 International Geoscience and Remote Sensing Symposium (Cat. No. 01CH37217). https://doi.org/10.1109/IGARSS.2001.976657

Klonus, S., & Ehlers, M. (2009). Performance of evaluation methods in image fusion. 2009 12th international conference on information fusion,

Kwarteng, P., & Chavez, A. (1989). Extracting spectral contrast in Landsat Thematic Mapper image data using selective principal component analysis. Photogramm. Eng. Remote Sens, 55(1), 339-348. https://doi.org/0099-1112/89/5503-339$02.25/0

Laben, C., & Brower, B. (2000). US Patent No. 6,011,875. US Patent.

Laben, C. A., & Brower, B. V. (2000). Process for enhancing the spatial resolution of multispectral imagery using pan-sharpening. In: Google Patents.

Lari, S. N., & Yazdi, M. (2016). Improved IHS pan-sharpening method based on adaptive injection of à trous wavelet decomposition. International Journal of Signal Processing, Image Processing and Pattern Recognition, 9(3), 291-308. https://doi.org/10.14257/ijsip.2016.9.3.26

Li, H., Jing, L., & Tang, Y. (2017). Assessment of pansharpening methods applied to WorldView-2 imagery fusion. Sensors, 17(1), 89. https://doi.org/10.3390/s17010089

Li, N., Huang, N., & Xiao, L. (2017). Pan-sharpening via residual deep learning. 2017 IEEE international geoscience and remote sensing symposium (IGARSS). https://doi.org/10.1109/IGARSS.2017.8128158

Li, X., Zhang, Y., Gao, Y., & Yue, S. (2016). Using guided filtering to improve gram-schmidt based pansharpening method for geoeye-1 satellite images. 4th International Conference on Information Systems and Computing Technology. https://doi.org/10.2991/isct-16.2016.6

Licciardi, G., Vivone, G., Mura, M. D., Restaino, R., & Chanussot, J. (2016). Multi-resolution analysis techniques and nonlinear PCA for hybrid pansharpening applications. Multidimensional Systems and Signal Processing, 27, 807-830.

https://doi.org/10.1007/s11045-015-0359-y

Liu, J. (2000). Smoothing filter-based intensity modulation: A spectral preserve image fusion technique for improving spatial details. International Journal of remote sensing, 21(18), 3461-3472. https://doi.org/10.1080/014311600750037499

Liu, Q., Zhou, H., Xu, Q., Liu, X., & Wang, Y. (2020). PSGAN: A generative adversarial network for remote sensing image pan-sharpening. IEEE Transactions on Geoscience and Remote Sensing, 59(12), 10227-10242. https://doi.org/10.48550/arXiv.1805.03371

Masi, G., Cozzolino, D., Verdoliva, L., & Scarpa, G. (2016). Pansharpening by convolutional neural networks. Remote Sensing, 8(7), 594. https://doi.org/10.3390/rs8070594

Nunez, J., Otazu, X., Fors, O., Prades, A., Pala, V., & Arbiol, R. (1999). Multiresolution-based image fusion with additive wavelet decomposition. IEEE Transactions on Geoscience and Remote Sensing, 37(3), 1204-1211. https://doi.org/10.1109/36.763274

Palsson, F., Sveinsson, J. R., & Ulfarsson, M. O. (2013). A new pansharpening algorithm based on total variation. IEEE Geoscience and Remote sensing letters, 11(1), 318-322. https://doi.org/10.1109/LGRS.2013.2257669

Palsson, F., Ulfarsson, M. O., & Sveinsson, J. R. (2019). Model-based reduced-rank pansharpening. IEEE Geoscience and Remote sensing letters, 17(4), 656-660. https://doi.org/10.1109/LGRS.2019.2926681

Pushparaj, J., & Hegde, A. V. (2017). Evaluation of pan-sharpening methods for spatial and spectral quality. Applied Geomatics, 9, 1-12. https://doi.org/10.1007/s12518-016-0179-2

Rahimzadeganasl, A., Alganci, U., & Goksel, C. (2019). An approach for the pan sharpening of very high resolution satellite images using a CIELab color based component substitution algorithm. Applied Sciences, 9(23), 5234. https://doi.org/10.3390/app9235234

Restaino, R. (2024). Pansharpening Techniques: Optimizing the Loss Function for Convolutional Neural Networks. Remote Sensing, 17(1), 16. https://doi.org/10.3390/rs17010016

Restaino, R., Vivone, G., Dalla Mura, M., & Chanussot, J. (2016). Fusion of multispectral and panchromatic images based on morphological operators. IEEE Transactions on Image Processing, 25(6), 2882-2895. https://doi.org/10.1109/TIP.2016.2556944

Samadzadegan, F., Aghvami, M., Toosi, A., Hasani, H., Amini, O., & Ahadzadeh, S. (2025). On-orbit Spatial Resolution Assessment of Khayyam Satellite Imagery Using Natural Edge Targets. Advances in space research. https://doi.org/10.1016/j.asr.2025.07.101

Schavemaker, J. G., Reinders, M. J., Gerbrands, J. J., & Backer, E. (2000). Image sharpening by morphological filtering. Pattern Recognition, 33(6), 997-1012. https://doi.org/10.1016/S0031-3203(99)00160-0

Shah, V. P., Younan, N. H., & King, R. (2007). Pan-sharpening via the contourlet transform. 2007 IEEE International Geoscience and Remote Sensing Symposium. https://doi.org/10.1109/IGARSS.2007.4422792

Su, X., Li, J., & Hua, Z. (2022). Transformer-based regression network for pansharpening remote sensing images. IEEE Transactions on Geoscience and Remote Sensing, 60, 1-23. https://doi.org/10.1109/TGRS.2022.3152425

Tu, T.-M., Huang, P. S., Hung, C.-L., & Chang, C.-P. (2004). A fast intensity-hue-saturation fusion technique with spectral adjustment for IKONOS imagery. IEEE Geoscience and Remote sensing letters, 1(4), 309-312. https://doi.org/10.1109/LGRS.2004.834804

Tu, T.-M., Su, S.-C., Shyu, H.-C., & Huang, P. S. (2001). A new look at IHS-like image fusion methods. Information Fusion, 2(3), 177-186. https://doi.org/10.1016/S1566-2535(01)00036-7

Vivone, G., Alparone, L., Chanussot, J., Dalla Mura, M., Garzelli, A., Licciardi, G. A., Restaino, R., & Wald, L. (2014). A critical comparison among pansharpening algorithms. IEEE Transactions on Geoscience and Remote Sensing, 53(5), 2565-2586. https://doi.org/10.1109/TGRS.2014.2361734

Vivone, G., Simões, M., Dalla Mura, M., Restaino, R., Bioucas-Dias, J. M., Licciardi, G. A., & Chanussot, J. (2014). Pansharpening based on semiblind deconvolution. IEEE Transactions on Geoscience and Remote Sensing, 53(4), 1997-2010. https://doi.org/10.1109/TGRS.2014.2351754

Wady, S., Bentoutou, Y., Bengermikh, A., Bounoua, A., & Taleb, N. (2020). A new IHS and wavelet based pansharpening algorithm for high spatial resolution satellite imagery. Advances in space research, 66(7), 1507-1521. https://doi.org/10.1016/j.asr.2020.06.001

Wald, L. (2000). Quality of high resolution synthesised images: Is there a simple criterion? Third conference" Fusion of Earth data: merging point measurements, raster maps and remotely sensed images",

Wald, L., Ranchin, T., & Mangolini, M. (1997). Fusion of satellite images of different spatial resolutions: Assessing the quality of resulting images. Photogrammetric Engineering and remote sensing, 63(6), 691-699.

Wang, J., Shao, Z., Huang, X., Lu, T., Zhang, R., & Cheng, G. (2022). Pan-sharpening via deep locally linear embedding residual network. IEEE Transactions on Geoscience and Remote Sensing, 60, 1-13. https://doi.org/10.1016/j.jag.2024.104045

Wang, P., Yao, H., Huang, B., Leung, H., & Liu, P. (2023). Multiresolution analysis pansharpening based on variation factor for multispectral and panchromatic images from different times. IEEE Transactions on Geoscience and Remote Sensing, 61, 1-17. https://doi.org/10.1109/TGRS.2023.3252001

Wang, S., Zou, X., Li, K., Xing, J., Cao, T., & Tao, P. (2024). Towards robust pansharpening: A large-scale high-resolution multi-scene dataset and novel approach.

Remote Sensing, 16(16), 2899. https://doi.org/10.3390/rs16162899

Wang, Z., & Bovik, A. C. (2002). A universal image quality index. IEEE signal processing letters, 9(3), 81-84. https://doi.org/10.1109/97.995823

Wang, Z., Bovik, A. C., Sheikh, H. R., & Simoncelli, E. P. (2004). Image quality assessment: from error visibility to structural similarity. IEEE Transactions on Image Processing, 13(4), 600-612. https://doi.org/10.1109/TIP.2003.819861

Wu, J., Lin, L., Zhang, C., Li, T., Cheng, X., & Nan, F. (2023). Generating Sentinel-2 all-band 10-m data by sharpening 20/60-m bands: A hierarchical fusion network. ISPRS journal of photogrammetry and remote sensing, 196, 16-31. https://doi.org/10.1016/j.isprsjprs.2022.12.017

Xu, Q., Zhang, Y., & Li, B. (2014). Recent advances in pansharpening and key problems in applications. International Journal of Image and Data Fusion, 5(3), 175-195. https://doi.org/10.1080/19479832.2014.889227

Yang, J., Fu, X., Hu, Y., Huang, Y., Ding, X., & Paisley, J. (2017). PanNet: A deep network architecture for pan-sharpening. Proceedings of the IEEE international conference on computer vision. https://doi.org/10.1109/ICCV.2017.193

Zhao, Q., Yu, L., Du, Z., Peng, D., Hao, P., Zhang, Y., & Gong, P. (2022). An overview of the applications of earth observation satellite data: impacts and future trends. Remote Sensing, 14(8), 1863. https://doi.org/10.3390/rs14081863

Zhou, Z., Ma, N., Li, Y., Yang, P., Zhang, P., & Li, Y. (2014). Variational PCA fusion for Pan-sharpening very high resolution imagery. Science China Information Sciences, 57, 1-10. https://doi.org/10.1007/s11432-014-5108-6